JBC RESEARCH ARTICLE

# The molecular basis of the inhibition of $Ca_V1$ calcium-dependent inactivation by the distal carboxy tail

Received for publication, December 29, 2020, and in revised form, February 25, 2021 Published, Papers in Press, March 2, 2021, https://doi.org/10.1016/j.jbc.2021.100502

**Lingjie Sang[1], Daiana C. O. Vieira[2], David T. Yue[1], Manu Ben-Johny[1,3], and Ivy E. Dick[1,2,*]**

*From the [1]Department of Biomedical Engineering, The Johns Hopkins University School of Medicine, Baltimore, Maryland, USA; [2]Department of Physiology, University of Maryland School of Medicine, Baltimore, Maryland, USA; [3]Department of Physiology and Cellular Biophysics, Columbia University, New York, New York, USA*

Edited by Mike Shipston

**$Ca^{2+}$/calmodulin-dependent inactivation (CDI) of $Ca_V$ channels is a critical regulatory process that tunes the kinetics of $Ca^{2+}$ entry for different cell types and physiologic responses. CDI is mediated by calmodulin (CaM), which is bound to the IQ domain of the $Ca_V$ carboxy tail. This modulatory process is tailored by alternative splicing such that select splice variants of $Ca_V1.3$ and $Ca_V1.4$ contain a long distal carboxy tail (DCT). The DCT harbors an inhibitor of CDI (ICDI) module that competitively displaces CaM from the IQ domain, thereby diminishing CDI. While this overall mechanism is now well described, the detailed interactions required for ICDI binding to the IQ domain are yet to be elucidated. Here, we perform alanine-scanning mutagenesis of the IQ and ICDI domains and evaluate the contribution of neighboring regions to CDI inhibition. Through FRET binding analysis, we identify functionally relevant residues within the $Ca_V1.3$ IQ domain and the $Ca_V1.4$ ICDI and nearby A region, which are required for high-affinity IQ/ICDI binding. Importantly, patch-clamp recordings demonstrate that disruption of this interaction commensurately diminishes ICDI function resulting in the re-emergence of CDI in mutant channels. Furthermore, $Ca_V1.2$ channels harbor a homologous DCT; however, the ICDI region of this channel does not appear to appreciably modulate $Ca_V1.2$ CDI. Yet coexpression of $Ca_V1.2$ ICDI with select $Ca_V1.3$ splice variants significantly disrupts CDI, implicating a cross-channel modulatory scheme in cells expressing both channel subtypes. In all, these findings provide new insights into a molecular rheostat that fine-tunes $Ca^{2+}$-entry and supports normal neuronal and cardiac function.**

L-type voltage-gated calcium channels ($Ca_V1.1$–$1.4$) are an important conduit for extracellular $Ca^{2+}$ entry into many excitable cells including cardiac myocytes, neurons, smooth muscle, and skeletal muscle (1–4). As such, these channels are subject to rich and powerful modes of feedback regulation (5–7). In particular, $Ca^{2+}$/calmodulin-dependent inactivation (CDI) of L-type channels is a crucial negative feedback mechanism that reshapes the electrical properties of neurons and cardiac myocytes and protects cells from $Ca^{2+}$ overload (8–10). CDI is driven by the ubiquitous $Ca^{2+}$ sensing molecule, calmodulin (CaM) (10, 11). Under basal $Ca^{2+}$ conditions, $Ca^{2+}$-free CaM (apoCaM) binds to the carboxy-terminal IQ domain of the channel and enhances channel openings (12). Upon elevation of intracellular $Ca^{2+}$, the "resident" CaM repositions on the channel, interacting with $Ca^{2+}$/CaM binding sites located on the channel amino- and proximal carboxy- termini (13, 14). This conformational change antagonizes the initial upregulation in channel open probability, which manifests as CDI. Not surprisingly, CDI of L-type channels has emerged as a key physiological process to limit excess $Ca^{2+}$ influx during repetitive or sustained depolarization, and disruption of this feedback in the cardiac myocytes may lead to lethal cardiac arrhythmias (15, 16). This stereotypic behavior, however, diverges in multiple physiological settings where strong CDI of L-type channels is curtailed, thus permitting $Ca^{2+}$ channels to faithfully respond to a tonic stimulus. For example, in photoreceptors and bipolar cells, endogenous $Ca_V1.4$ exhibits minimal CDI, thereby allowing sustained $Ca^{2+}$ influx and slow, graded changes in the membrane potential necessary for tonic glutamate release, and normal vision (17, 18). Similarly, $Ca_V1.3$ channels in inner hair cells also lack CDI (19). Beyond these, the basal strength of $Ca_V1.2$ and $Ca_V1.3$ CDI varies in different neuronal subtypes in the central nervous system, suggesting a sophisticated scheme of $Ca_V$ channel feedback ripe with physiological insights (20).

The molecular mechanisms that fine-tune L-type channel CDI are twofold and have been of long-standing interest. One scheme involves channel-interacting proteins such as calmodulin-like $Ca^{2+}$-binding proteins (CaBP1-4) (18, 19, 21, 22) and SH3 and cysteine-rich domain containing proteins (stac1-3) (23–26) that suppress CDI utilizing an allosteric or mixed-allosteric mechanism. In contrast, $Ca_V1.3$ and $Ca_V1.4$ channels may intrinsically disable CDI *via* an alternatively spliced specialized CDI-inhibiting module (ICDI) within the distal carboxy tail (DCT) of the channel (20, 27–33). The latter form of regulation is complex and bears important biological consequences. First, splice inclusion of the DCT occurs in a cell-type-dependent manner. For instance, alternative splicing of $Ca_V1.3$ results in variable inclusion of the ICDI domain in distinct regions of the brain and in the sinoatrial node, enabling precise tuning of CDI in these cell types (27, 31, 34, 35). Second, $Ca_V1.2$ appears to harbor a highly homologous

* For correspondence: Ivy E. Dick, ied@som.umaryand.edu.

ICDI region (33), yet CDI for this channel is known to be robust, both when evaluated as full-length channels in heterologous expression system and in primary cells where the carboxy-tail containing ICDI is believed to be cleaved off the channel (9–11, 33). As such, the function of the ICDI module within $Ca_V1.2$ channels remains unclear. Third, the inhibition of CDI by ICDI is the result of competitive binding by apoCaM *versus* ICDI with the channel IQ domain (20, 31). In addition to diminishing CDI, the displacement of apoCaM results in a dramatic decrease in baseline channel open probability (12). Fourth, adding to the richness the modulatory role of ICDI, RNA editing, and/or fluctuations in cytosolic CaM concentrations can tune the extent of this competition, enabling different degrees of CDI tailored to specific cell types or physiologic states (12, 36). Importantly, pathologic changes to this system may be linked to altered CaM concentrations in Parkinson's disease and heart failure (37, 38), and mutations within the ICDI of $Ca_V1.4$ channels are known to be causative of congenital stationary night blindness (32, 39, 40). Thus, the modulation of CDI by ICDI stands as a critical and robust mechanism for adapting channel regulation to select cell types and conditions. Moreover, as the number of known pathogenic mutations within LTCCs continues to grow, the ability to map these mutations to a locus with known mechanistic impact would enable rapid insight into the pathogenesis of LTCC channelopathies.

Although the overall competitive nature of ICDI regulation of L-type channels is now well established (20, 31), the precise binding interfaces involved in this regulation are yet to be identified. This gap in understanding is critical as mutations in the carboxy tail of LTCCs result in neurological disease (32, 39, 40). Furthermore, a residue-level analysis may shed light upon structural differences between the ICDI domain of $Ca_V1.3$ and the homologous segment of $Ca_V1.2$ that engender differential functional regulation. To characterize the landscape of the IQ/ICDI interaction of L-type channels, here we undertook systematic alanine scanning mutagenesis of both IQ and ICDI domains. Through live-cell FRET two-hybrid binding assays and electrophysiological analysis, we identified several novel hotspots on both IQ and ICDI segments that mediate a high-affinity interaction and are functionally relevant for CDI inhibition. Systematic analysis of these mutations revealed a strong inverse correlation between the strength of CDI and the binding affinity of the ICDI domain for the IQ segment, as predicted for a competitive inhibitor (13, 14, 20). Thus, we have identified residues that alter binding in a functionally relevant manner. Moreover, similar critical residues were identified in adjacent regions, defining a comprehensive interface map of the IQ/ICDI interaction. Finally, extending our analysis to $Ca_V1.2$ channels, we found that the ICDI module binds to the $Ca_V1.2$ IQ domain with a reduced affinity and that this binding is insufficient to cause more than a nominal change in the CDI of full-length channels. However, the ICDI from $Ca_V1.2$ is capable of binding the $Ca_V1.3$ IQ region with high affinity, resulting in a much larger decrease in CDI of these channels. Given the propensity of the carboxy tail of $Ca_V1.2$ to exist as a separate peptide within myocytes and neurons (27, 33, 41, 42), these findings raise the prospect of a cross-channel feedback scheme in some cell types. Overall, these results elucidate the detailed binding interface between components of the carboxy tail of L-type $Ca^{2+}$ channels, lending new insight into normal and pathologic channel regulation.

## Results

### *Identification of critical residues within the IQ domain necessary for ICDI binding*

To identify key residues that support a high-affinity IQ/ICDI interaction, we undertook systematic alanine substitution of the IQ domain and evaluated both the relative binding affinity and the strength of ICDI-mediated inhibition of CaM regulation. Importantly, the ICDI domains of both $Ca_V1.3$ and $Ca_V1.4$ are highly homologous and have been shown to interact with IQ domains in a similar manner evoking similar functional effects (20, 27, 29). Even so, the ICDI domain from $Ca_V1.4$ ($ICDI_{1.4}$) has a greater binding affinity for the IQ domains of both $Ca_V1.3$ and $Ca_V1.4$, with FRET binding assays yielding more robust measurements with enhanced signal-to-noise ratio as compared with $ICDI_{1.3}$ (43). We therefore focus on this canonical ICDI motif for our studies. However, robust expression of the holo-$Ca_V1.4$ channel in recombinant systems is notoriously challenging, largely due to their diminutive open probability (12, 44). We therefore chose to explore the interaction between the IQ domain of $Ca_V1.3$ channels ($IQ_{1.3}$) and $ICDI_{1.4}$. To this end, we utilized a chimeric channel in which the DCT of $Ca_V1.4$ is spliced onto the backbone of $Ca_V1.3$ ($Ca_V1.3_{\Delta/DCT1.4}$) (Fig. 1*A*), which has previously proven useful in dissecting the mechanisms underlying ICDI modulation of the channel (12, 20). This chimera furnishes a strong IQ/ICDI interaction coupled with a robust functional readout, enabling quantitative analysis.

To begin, we confirm the functional impact of ICDI in our chimeric channel by evaluating the extent of CDI in HEK293 cells. Indeed, CDI is entirely abolished in $Ca_V1.3_{\Delta/DCT1.4}$, as seen by the identical $Ba^{2+}$ and $Ca^{2+}$ current decay in response to a depolarizing pulse (Fig. 1*B*). However, removal of $DCT_{1.4}$ restores robust CDI, as seen by the rapid decay of the $Ca^{2+}$ current (Fig. 1*C*, red). In contrast, when $Ba^{2+}$ (which binds poorly to CaM) is used as the charge carrier, there is minimal inactivation (Fig. 1*C*, black). We therefore define the extent of CDI as the ratio of $Ca^{2+}$ current remaining after 300 ms of depolarization *versus* $Ba^{2+}$ current at the same time point.

We next utilized a FRET 2-hybrid binding assay (45, 46) to evaluate the relative strength of interactions between the IQ and ICDI regions. FRET binding pairs were constructed by tagging Cerulean fluorescent protein to $ICDI_{1.4}$, and Venus fluorescent protein to $PreIQ_3$-IQ-$A_{1.3}$, a peptide that includes $IQ_{1.3}$ as well as ∼30 residues upstream ($PreIQ_3$) and ∼150 residues downstream (A-region) of the IQ domain (Fig. 1*D*, Fig. S1). Both $PreIQ_3$ and A regions were included initially to ensure that all likely interacting residues were included. Strong binding was detected between the Venus-$PreIQ_3$-IQ-$A_{1.3}$ and Cerulean-$ICDI_{1.4}$, as can be appreciated by the steep FRET

binding curve determined by the FRET Ratio (FR) of each cell plotted as a function of the free donor concentration (Cerulean tagged $ICDI_{1.4}$) (Fig. 1*D*, *black*). After calibration, the FRET binding curve for WT Venus-$PreIQ_3$-IQ-$A_{1.3}$ *versus* Cerulean-$ICDI_{1.4}$ yielded a $K_a$ of 21.4 $\mu M^{-1}$. To identify key residues that support a high-affinity IQ/ICDI interaction, we undertook systematic alanine substitution of the IQ domain and evaluated the effect on binding affinity in our FRET assay. Within $IQ_{1.3}$, we substituted each residue with an alanine or, at loci where the wild-type channel featured an alanine, we replaced the residue with a threonine. For identification of each residue, the canonical isoleucine is assigned position 0. Application of our FRET assay to each mutated peptide identified three residues, Y[−5]A, F[−2]A, and F[+4]A, which severely perturbed the IQ/ICDI interaction (Fig. 1*E*, Fig. S1). Focusing on F[−2]A, FRET binding produced a shallower curve as compared with WT (Fig. 1*D*, *blue versus gray*), resulting in a $K_a$ of 5.8 $\mu M^{-1}$ (Fig. 1*E*, *blue*). Introducing this mutation into the chimeric channel resulted in a partial rescue of CDI (Fig. 1*F*), indicating that this interaction site is functionally relevant. However, the IQ domain substitutions Y[−5]A and F[+4]A, which also had a marked effect on $K_a$, resulted in minimal CDI rescue (Fig. 1, *F* and *G*, Fig. S2). Importantly, these residues also serve as anchors for apoCaM binding to the $Ca_V1.3$ IQ domain, resulting in weak baseline CDI even in the absence of the ICDI domain (Table S1) (13). Of note, this apoCaM effect may also underly the apparent increase in binding affinity demonstrated by several of the mutations, where a decrease in apoCaM binding would enhance the apparent binding of the IQ/ICDI regions due to altered competition with endogenous CaM.

In order to confirm the functional relevance of each binding loci identified, we turned to a previously described analysis known as individually transformed Langmuir (iTL) analysis (14). This approach allows us to rigorously correlate relative changes in binding with functional changes in CDI. As iTL was initially derived to evaluate the binding interfaces critical to CaM-mediated channel regulation (13, 14), we adjust the model to reflect the competitive binding scheme between CaM and ICDI (20). To do so, we first account for the ambiguity caused by binding sites, which are important for both apoCaM and ICDI binding. We therefore incorporate both the IQ domain's intrinsic affinity for apoCaM ($K_{a\text{-}CaM}$) and that for the ICDI segment ($K_{a\text{-}ICDI}$), the competitive inhibitor, by adjusting our measured $K_{a\text{-}ICDI}$ such that:

$$K^{corr}_{a-ICDI} = \frac{K^{WT}_{a-CaM}}{K^{mut}_{a-CaM}} \cdot K_{a-ICDI} \quad (1)$$

Where $K^{WT}_{a-CaM}$ is the apoCaM binding affinity of WT $PreIQ_3$-IQ-$A_{1.3}$, and $K^{mut}_{a-CaM}$ represents the apoCaM binding affinity of each mutant peptide, values which were previously measured (13) and are listed in Table S1. This compensation remains valid provided that the local concentration of ICDI is much greater than $K_{d\text{-}ICDI}$ ([ICDI]>> $1/K_{a\text{-}ICDI}$). With this adjustment made, CDI can be defined by a modified Langmuir function as follows:

$$\frac{CDI}{CDI_{max}} = \frac{[apoCaM]\cdot K_{a-CaM}}{1 + [apoCaM]\cdot K_{a-CaM} + [ICDI]\cdot K^{corr}_{a-ICDI}} \quad (2)$$

where *CDI* is the strength of CDI under endogenous levels of CaM; $CDI_{max}$ is the CDI in saturating concentrations of CaM (Table S1); $K_{a\text{-}CaM}$ is the association constant for apoCaM binding to $PreIQ_3$-IQ-$A_{1.3}$; [apoCaM] is the free apoCaM concentration in the cell; and [ICDI] is the effective local concentration of ICDI (see Supporting information for full derivation). Equation 2 predicts an inverse correlation between $K^{corr}_{a-ICDI}$ and relative *CDI*, which we can fit to our data (Fig. 1*H*). For channels containing WT $IQ_{1.3}$ and $ICDI_{1.4}$ domains, the strong binding between IQ and ICDI results in minimal CDI, as seen by the black data point on the plot. In contrast, $Ca_V1.3_\Delta$ channels, which lack an ICDI domain such that $K^{corr}_{a-ICDI} = 0$ by definition, display large CDI values (cyan). The F[−2]A mutation, which produced a partial restoration of CDI, resides in an intermediate position (blue). Overall, our data can be well fit by Equation 2 (Fig. 1*H*), confirming the functional relevance of the identified residues in a competitive model.

### *Alanine scanning of the ICDI domain reveals complementary hotspots*

Having identified several critical residues within the IQ domain required for ICDI binding, we next probed the ICDI for critical determinates of binding to the IQ. In order to scan a more extensive segment of the channel, we made triple alanine substitutions for every three contiguous residues within the ICDI domain. The ICDI domain has previously been localized to amino acids 1868 to 1956 of the $Ca_V1.3$ DCT (29, 32, 33). We therefore undertook our alanine scan on this segment of the channel. Importantly, this region includes the distal C-terminal regulatory domain (DCRD), which was previously identified as playing an important role in the ICDI-mediated inhibition of CDI (27, 31, 33, 47). Finally, we included a selective V[1907]A mutation, as this amino acid change has previously been shown to dramatically alter the function of ICDI (30). To evaluate the effect of these alanine substitutions on IQ/ICDI binding, we again utilized our FRET two-hybrid binding assay, pairing Venus-$PreIQ_3$-IQ-$A_{1.3}$ with Cerulean-$ICDI_{1.4}$ (Fig. 2*A*, Fig. S3). Indeed, measured $K_a$ values revealed multiple hotspots within the ICDI domain, with a wide range of binding affinities with the IQ containing peptide (Fig. 2*B*). Interestingly several mutations, largely toward either end of the peptide, appeared to modestly increase in $K_a$. However, these changes may reflect a structural stabilization of the isolated ICDI peptide by promoting helicity of end regions and may not necessarily yield a corresponding change in intact channels. As such, we did not pursue further analysis of these mutants. The two mutation sites displayed in gray (KQE[1911]AAA and YSD[1941]AAA) were not evaluated as they failed to express. Notably, the effects of the hotspots on the ICDI domain were significantly larger than those observed within the IQ domain (Fig. 2*B versus* Fig. 1*E*).

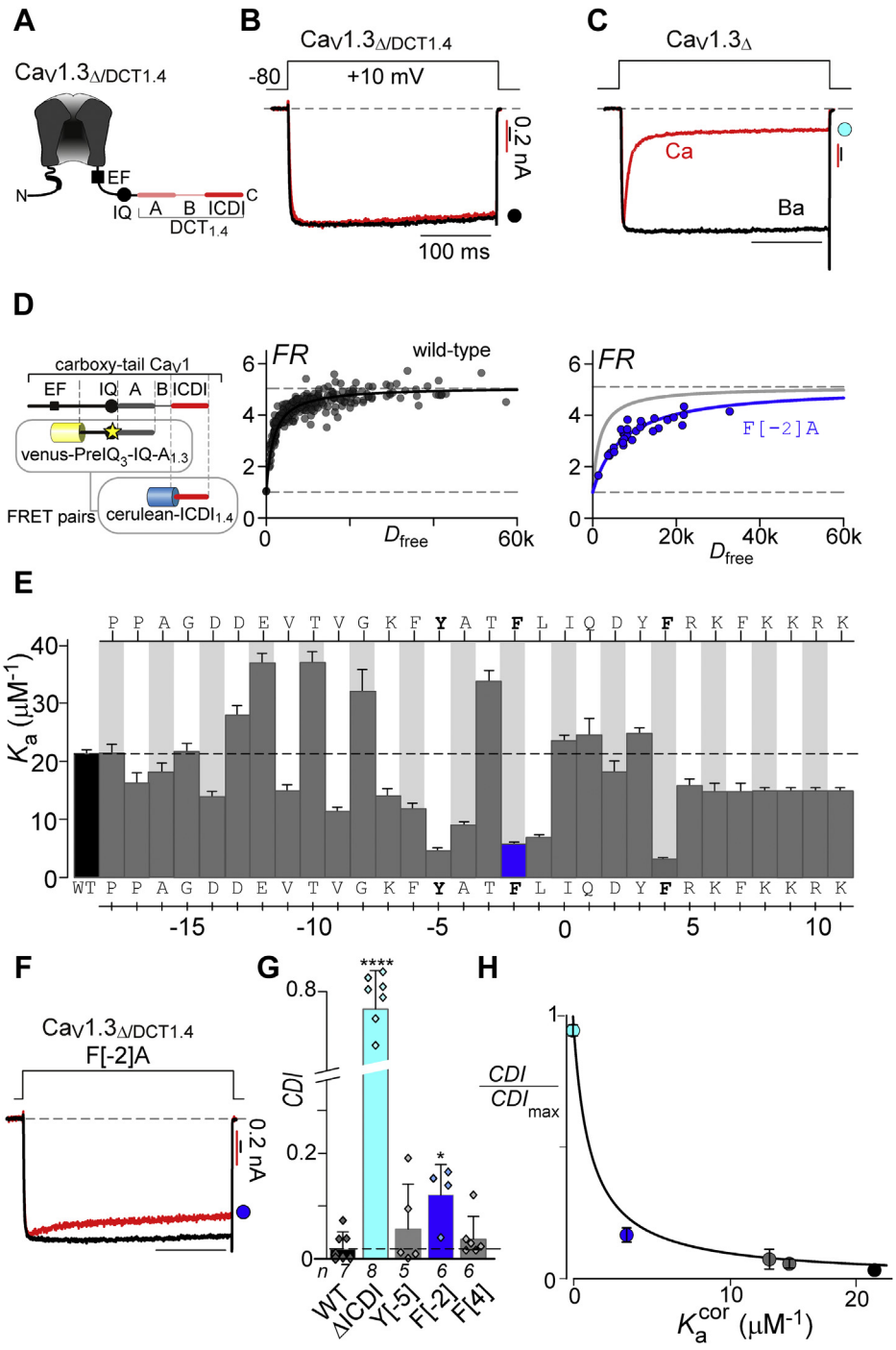


**Figure 1. Identifying the hotspots on the IQ region required for ICDI binding and function.** *A*, cartoon depicting the chimeric $Ca_V1.3_{\Delta/DCT1.4}$ channel. *B*, exemplar whole-cell recording showing minimal inactivation in response to a 10 mV step depolarization in $Ba^{2+}$ (*black*) or $Ca^{2+}$ (*red*) for $Ca_V1.3_{\Delta/DCT1.4}$ demonstrating the function of $ICDI_{1.4}$. $Ba^{2+}$ current is scaled to enable comparison of the kinetics of the two traces. *Red scale bar* refers to the $Ca^{2+}$ trace and *black* corresponds to the $Ba^{2+}$ trace here and throughout. *C*, exemplar whole-cell recording of the truncated $Ca_V1.3_{\Delta}$ channel, lacking the DCT containing ICDI. Robust CDI is seen as the strong decay of the $Ca^{2+}$ current (*red*) as compared to the $Ba^{2+}$ current. *D*, FRET two-hybrid assay of IQ/ICDI interaction. FRET binding partners are displayed on the *left*, with *star* indicating the locus of alanine mutations. Strong binding was measured for wild-type $preIQ_3$-IQ-$A_{1.3}$ with $ICDI_{1.4}$ (*black*), while the mutation F[−2]A (*blue*) decreased the binding affinity compared with WT (*gray*). *E*, summary of $K_a$ values for mutant Venus-$preIQ_3$-IQ-$A_{1.3}$ *versus* Cerulean-$ICDI_{1.4}$ peptides measured with FRET two-hybrid assay as in panel *D*. Alanine was systematically substituted into the IQ region of the Venus-$preIQ_3$-IQ-$A_{1.3}$ peptide, with the identity of the amino acid displayed on the *top* and *bottom of the bar graph* such that the canonical "I" of the IQ region is given position 0. The *dashed line* indicates the WT value and the *blue bar* corresponds to F[−2]A displayed in panel *D*. Data are displayed as mean ± SE. *F*, exemplar patch clamp data corresponding to F[−2]A in $Ca_V1.3_{\Delta/DCT1.4}$ demonstrating a partial recovery of CDI due to the mutation. *G*, average CDI values for each mutation, colors correspond to the data in other panels (ANOVA summary analysis indicates a likelihood of significant difference at a level of $p < 0.0001$. Post-hoc Dunnett's multiple comparisons *versus* WT indicated as ****$p < 0.0001$; *$p < 0.05$). Data is displayed as mean ± SD. *H*, CDI and binding data for the mutations is well fit by Equation 2, validating the competitive mechanism. *Colored circles* correspond to the colored data in the figure panels.

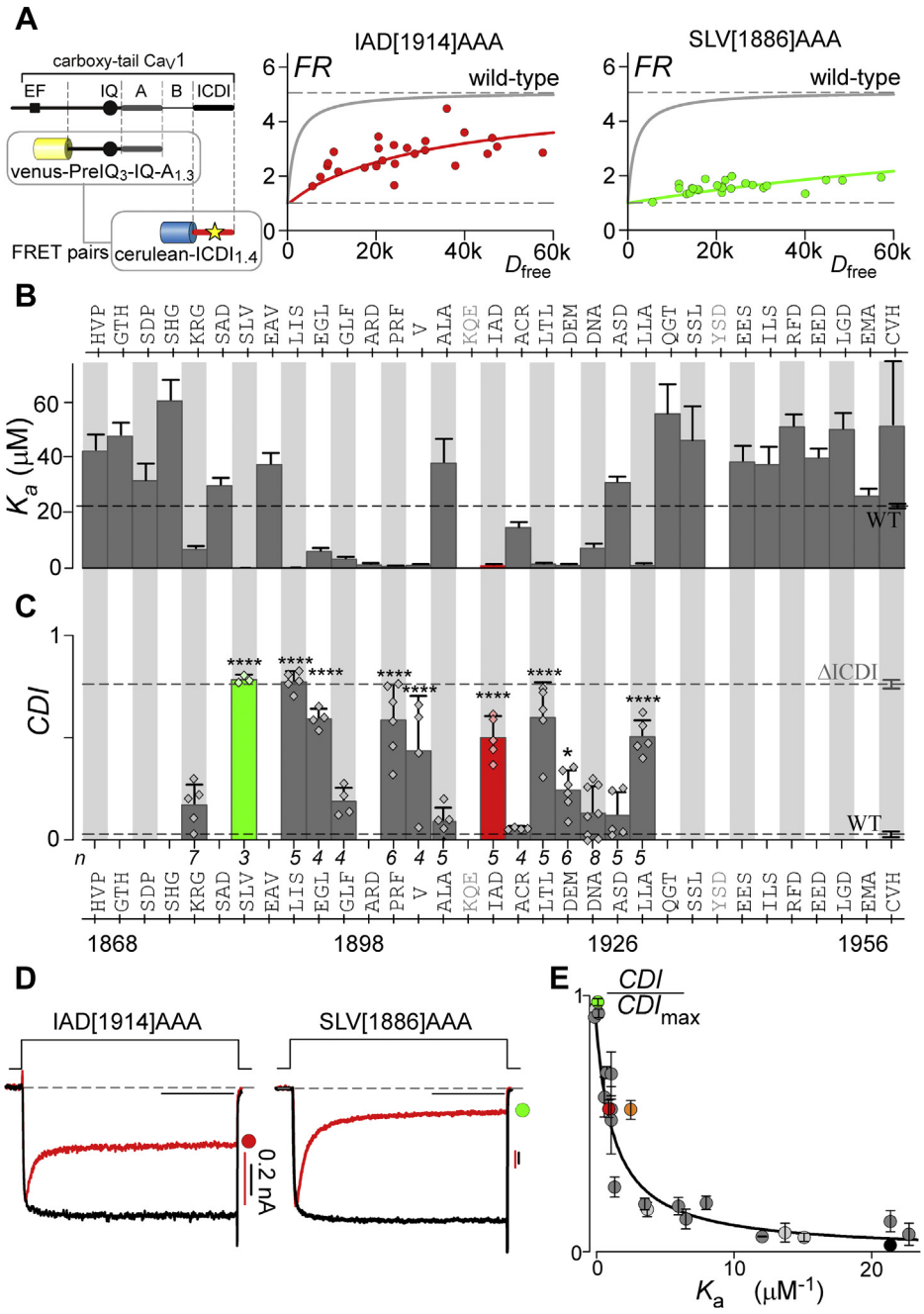


**Figure 2. Identifying the hotspots on $ICDI_{1.4}$ required for ICDI binding and function.** *A*, FRET binding partners are displayed on the *left*, with the *star* indicating the locus of alanine mutations within $ICDI_{1.4}$. Compared with WT (*gray line*), IAD[1914]AAA (*red*) and SLV[1886]AAA (*green*) significantly decreased binding affinity between the FRET pairs to differing degrees. *B*, summary of $K_a$ values for Venus-$PreIQ_3$-$IQA_{1.3}$ *versus* mutant Cerulean-$ICDI_{1.4}$ peptides measured with FRET two-hybrid as in panel *A*. Alanine was systematically substituted three amino acids at a time into Cerulean-$ICDI_{1.4}$, with the identity of the amino acids displayed on the *top of the bar graph*. Amino acids labeled in *gray* (KQE, YSD) were not evaluated due to poor expression. The *dashed line* indicates the WT value and the *colored bars* correspond to data in other panels of the figure here and throughout. Data are displayed ±SE. *C*, summary of CDI values measured for $Ca_V1.3_{\Delta/DCT1.4}$ harboring mutations corresponding to mutations that produced large effects on binding affinity in *B*. *Gray dashed line* represents the robust CDI of the channel without $ICDI_{1.4}$, while the *black dashed line* indicates the nominal CDI of WT $Ca_V1.3_{\Delta/DCT1.4}$. Data are displayed ±SD (ANOVA summary analysis indicates a likelihood of significant difference at a level of $p < 0.0001$. Post-hoc Dunnett's multiple comparisons *versus* WT indicated as ****$p < 0.0001$; *$p < 0.05$). *D*, exemplar whole-cell recordings of $Ca_V1.3_{\Delta/DCT1.4}$, demonstrating a significant restoration of CDI due to IAD[1914]AAA and near complete CDI due to SLV[1886]AAA. *E*, robust fit of CDI (*C*) and FRET binding data (*B*) to Equation 2, using identical parameters as in Figure 1*H*. *Light gray circles* indicate data from Figure 1, while *dark gray* and *colored circles* indicate mutations within ICDI corresponding to *B* and *C*, with *green* and *red circles* indicating exemplars shown in other panels for reference. The PKA phosphorylation site Ser1883 is plotted as the *orange circle*.

In order to correlate loss of binding affinity with function, we measured the CDI of those mutations that exhibited a large change in binding affinity (Fig. 2*C*, Fig. S4). As predicted, mutations that resulted in a significant loss of IQ/ICDI binding also exhibited a corresponding restoration of CDI. Focusing on two examples, IAD[1914]AAA moderately reduced IQ/ICDI

binding (Fig. 2, *A* and *B*, *red*), while introduction of the same mutations into our chimeric channel enabled a partial restoration of CDI (Fig. 2, *C* and *D*, *red*). On the other hand, SLV [1886]AAA displayed a drastic reduction in IQ/ICDI binding (Fig. 2, *A* and *B green*), and CDI was fully restored to the level seen in $Ca_V1.3_{\Delta}$ (Fig. 2, *C* and *D green*). Importantly, all identified loci are well fit by our Langmuir function, such that the same set of Equation 2 parameters describes both the IQ region and ICDI (Fig. 2*E*). Of note, as mutations in ICDI do not affect the binding of apoCaM, the correction factor for $K_a$ is no longer required, and $K^{corr}_{a-ICDI} = K_{a-ICDI}$. Having identified critical loci within ICDI, we note that one of these amino acids (S[1866]) has previously been identified as a phosphorylation site, which reduces the binding affinity of $ICDI_{1.4}$ by about tenfold, while increasing CDI of $Ca_V1.3_{\Delta/DCT1.4}$ (43). We therefore included the results of phosphorylation at this site in our analysis (Fig. 2*E*, *orange*). Indeed, phosphorylation of this amino acid results in a change in binding affinity, which correlates with CDI according to the same Langmuir function. Thus, we have identified numerous residues within $ICDI_{1.4}$, which are critical determinants of a functional competition between ICDI and apoCaM for the IQ region of $Ca_V1.3$.

### *The role of the A region in the IQ/ICDI interaction*

While our analysis identified several functionally relevant IQ domain loci, the impact of these mutations was far less than those identified within the ICDI (Fig. 1 *versus* Fig. 2). This suggests that additional regions outside the IQ domain may contribute to ICDI binding. In order to identify such regions, we generated truncated variations of our Venus-$PreIQ_3$-IQ-$A_{1.3}$ construct and paired them with Cerulean-$ICDI_{1.4}$ in the FRET two-hybrid binding assays (Fig. 3*A*, Fig. S5). We began by removing the $PreIQ_3$, and found no change in FRET binding, indicating that all relevant interaction loci are contained within the IQ and A regions (Fig. 3*B*, *blue*). However, removal of the IQ domain, leaving only the A region intact, resulted in a complete loss of FRET binding (Fig. 3*B*, *open circles*). Likewise, the IQ region alone displayed no binding

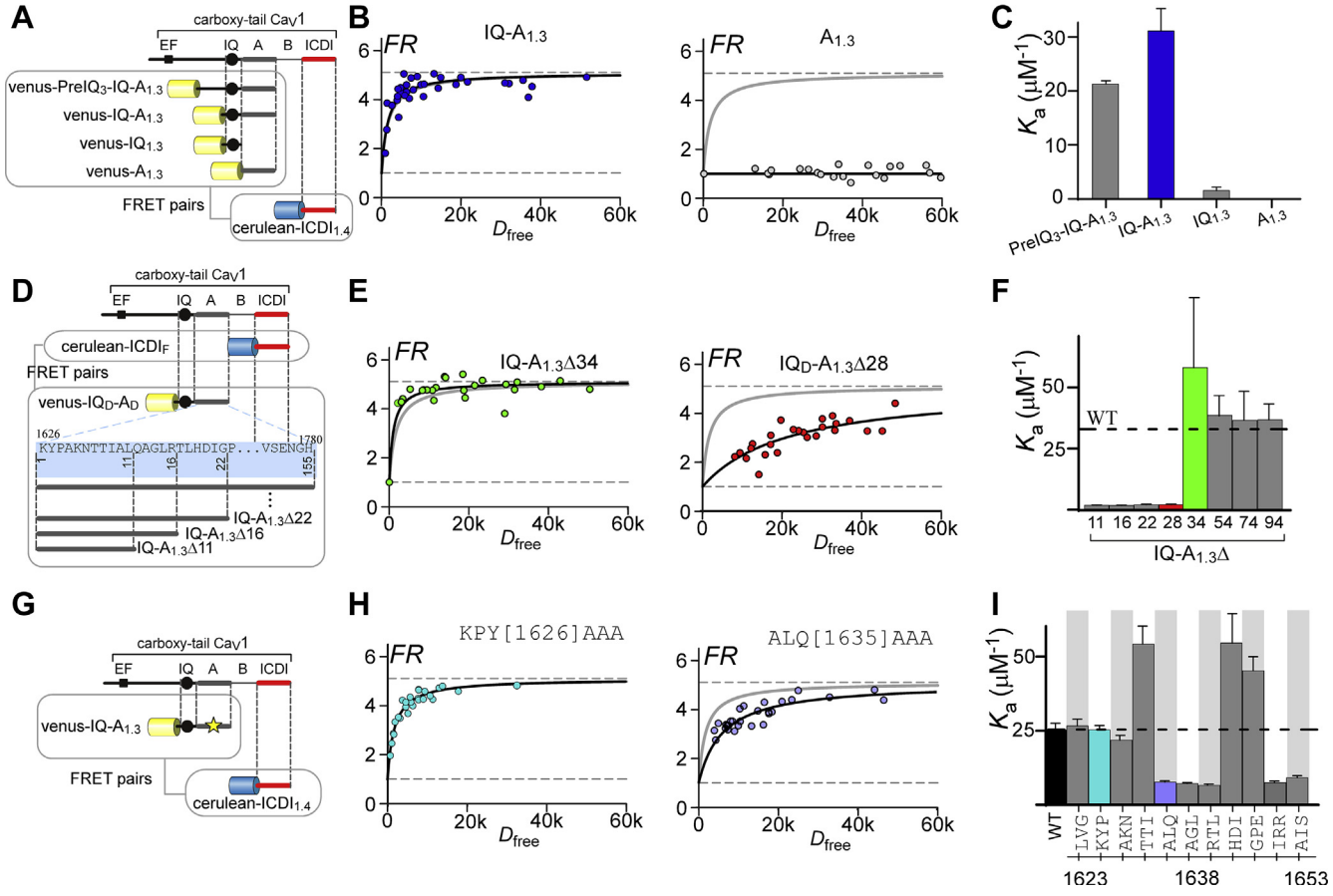


**Figure 3. Elucidating the role of the A region for ICDI interaction.** *A*, cartoon depicting FRET interacting pairs for panels *B* and *C*. Portions of the $PreIQ_3$-IQ-$A_{1.3}$ were paired with $ICDI_{1.4}$ to identify critical regions. *B*, IQ-$A_{1.3}$ is sufficient to support robust FRET (*blue*), indicating that the pre-$IQ_3$ region is not involved in the interaction. However, the A region alone is not sufficient to support binding (*open circles*). *C*, $K_a$ values for each channel fragment indicate that neither $IQ_{1.3}$ nor $A_{1.3}$ is sufficient for robust binding with $ICDI_{1.4}$; however, both regions are necessary as indicated by the robust binding of IQ-$A_{1.3}$ with $ICDI_{1.4}$. Data are displayed as mean ± SE here and throughout. *D*, cartoon depicting FRET interacting pairs for panels *E* and *F*. Cerulean-$ICDI_{1.4}$ was paired with various truncations of Venus-$PreIQ_3$-IQ-$A_{1.3}$. The *blue box* shows the sequence of the A region and illustrates the truncation strategy. *E* and *F*, truncating up to 34 amino acids distal to the IQ region (Δ34) had nominal effects on binding (*green*); however, removal of six additional amino acids (Δ28) dramatically reduced binding affinity (*red*). *G*, cartoon depicting FRET interacting pairs for panels *H* and *I*. Alanine substitutions were made within the A region, as indicated by the *yellow star*. *H*, mutation of KPY[1626]AAA within the A region had no effect on binding (*cyan*), while ALQ[1635]AAA (*purple*) diminished the binding affinity between IQ-$A_{1.3}$ and $ICDI_{1.4}$. *I*, summary of $K_a$ values for alanine mutations in the A region indicate multiple critical amino acids.

with ICDI (Fig. 3*C*), suggesting that both the IQ and the A region are necessary for interaction with ICDI. In order to further localize the critical interaction sites, we undertook successive truncation of the vernus-IQ-$A_{1.3}$ peptide (Fig. 3*D*). FRET measurements demonstrated minimal effect of truncations up to 34 amino acids from the end of the A region, as demonstrated by the strong binding of Venus-IQ-$A_{1.3}\Delta34$ with $ICDI_{1.4}$ (Fig. 3*E*, *green*). However, our next truncation, Venus-IQ-$A_{1.3}\Delta28$, exhibited a marked decrease in FRET binding (Fig. 3, *E* and *F*, *red*) Thus, the 34 residues immediately downstream of the IQ domain critically augment ICDI binding. Of note, this region includes the previously identified proximal C-terminal regulatory domain (PCRD), which is reported to play an important role in the ICDI interaction (27, 31, 33, 47). Having identified a subset of the A region, which is vital to ICDI binding, we again undertook systematic alanine substitutions, replacing each of the three contiguous residues with three alanine residues and undertook our FRET-2-hybrid binding assay (Fig. 3*G*). Disruptions in binding were identified as the result of a number of mutations, spanning both the previously identified PCRD region and a previously unidentified region upstream of this motif (Fig. 3, *H* and *I*, Fig. S6). Thus, both the IQ and the distal A region of the channel are required for high-affinity interaction with ICDI.

### *The functional relevance of ICDI in $Ca_V1.2$ channels*

Similar to $Ca_V1.3$ and $Ca_V1.4$, $Ca_V1.2$ channels also feature a highly homologous ICDI segment, argued to function as a channel inhibitor (33, 48) or as a transcriptional factor (41, 42). We therefore considered the impact of $ICDI_{1.2}$ on both $Ca_V1.2$ and $Ca_V1.3$ channels. We interrogated the binding of Cerulean-$ICDI_{1.2}$ with Venus-$PreIQ_3$-IQ-$A_{1.2}$ *via* FRET two-hybrid (Fig. 4, *A* and *B*) and found that the interaction is significantly weaker than the prototypic Venus-$PreIQ_3$-IQ-$A_{1.2}$ and Cerulean-$ICDI_{1.4}$ interaction (Fig. 4*B versus* Fig. 1*D*). However, when paired with Venus-$PreIQ_3$-IQ-$A_{1.3}$, binding with $ICDI_{1.2}$ is significantly larger, and only about half that of the strong binding of $ICDI_{1.4}$ (Fig. 4*C*). Thus, it appears that $ICDI_{1.2}$ is poised to have a larger effect in the context of $Ca_V1.3$ channels as compared with its native channel backbone. Nonetheless, the limited binding observed between Cerulean-$ICDI_{1.2}$ and Venus-$PreIQ_3$-IQ-$A_{1.2}$ prompted us to evaluate the possibility of a functional role for $ICDI_{1.2}$ within $Ca_V1.2$ channels. Interestingly, truncation of $Ca_V1.2$ at the known carboxy-tail cleavage site (49) for this channel ($Ca_V1.2_{\Delta1800}$) resulted in a minimal, yet statistically significant ($p \leq 0.05$), increase in CDI (Fig. 4, *D* and *F*, Fig. S7). Next, to test the effect of $ICDI_{1.2}$ on $Ca_V1.3$ channels, we replaced the native $ICDI_{1.3}$ of $Ca_V1.3_{long}$ channels with $ICDI_{1.2}$. Indeed, the loss of CDI surpassed that of $Ca_V1.2$ channels (Fig. 4*E*), as predicted based on the stronger $PreIQ_3$-IQ-$A_{1.3}$/$ICDI_{1.2}$ interaction (Fig. 4*C*). In fact, the CDI exhibited by $Ca_V1.3$-$ICDI_{1.2}$ channels was not statistically different than the CDI measured in the native $Ca_V1.3_{long}$ splice variant (Fig. 4*F*).

Multiple studies have shown that the DCT of $Ca_V1.2$, containing $ICDI_{1.2}$, exists as a peptide within neurons and cardiomyocytes, either due to proteolysis (33, 49) or as a result of alternative transcriptional initiation sites (41). Moreover, it has previously been demonstrated that ICDI domains can exert their effects on L-type channels when expressed as separate peptides (27). We therefore sought to recreate the potential interaction of select $Ca_V1.3$ channel variants with the DCT of $Ca_V1.2$. To begin, we choose the human $Ca_V1.3_{43S}$ splice variant of $Ca_V1.3$, as these channels terminate just past the A region and thus lack an inherent ICDI module (27). In addition, the inclusion of the A region within $Ca_V1.3_{43S}$ has been demonstrated to be important for ICDI binding, both in functional experiments done by others (27) and in our alanine scan of the A region (Fig. 3). We therefore generated the proteolytic product of human $Ca_V1.2$ channels ($DCT_{1.2}$) and evaluated the effect of this peptide on the CDI of $Ca_V1.3_{43S}$. Indeed, consistent with previous studies (27), coexpression of $DCT_{1.2}$ significantly reduced the CDI of $Ca_V1.3_{43S}$ (Fig. 4*G*, Fig. S7). For comparison, we also coexpressed these channels with $ICDI_{1.4}$ expressed as a peptide, which we have shown has a $K_a$ about double that of $ICDI_{1.2}$ (Fig. 4*C versus* Fig. 1*D*). Indeed, $ICDI_{1.4}$ results in an even larger CDI deficit when expressed with $Ca_V1.3_{43S}$ (Fig. 4, *G* and *H*). Thus, the proteolytically cleaved $DCT_{1.2}$ is well poised to exert a significant modulation of select $Ca_V1.3$ channel variants, such that the ambient concentrations of CaM and $DCT_{1.2}$ are able to tune the CDI of $Ca_V1.3_{43S}$ channels in a competitive manner (Fig. 4*I*).

## Discussion

CaM regulation of $Ca_V$ channels is vital to normal physiology and thus has been the subject of intense study (8, 10, 11, 17, 50–52). The competitive mechanism of ICDI within select $Ca_V1$ channels forms a basis with which CaM regulation can be tuned (12, 20, 32). Numerous processes designed to modulate this regulation include splice variation, RNA editing, variations in ambient CaM concentration, and phosphorylation (12, 13, 18, 36, 43). Identification of critical loci involved in this regulation is therefore key to understanding how CaM regulation may vary in different physiological and pathological states. As such, in-depth residue-level analysis not only reveals interfaces utilized by cells to tune channel regulation, but may offer targets in the search for novel regulators of the channel, which may have therapeutic benefit. In particular, the dramatically different efficacy of ICDI across channel subtypes may offer the possibility of subtype selective drug targeting, which remains challenging for $Ca_V1$ channels.

Given the importance of understanding these interactions within the carboxy-tail of $Ca_V1$ channels, we quantified the structure–function relationship of these interactions using a variant of previously described iTL analysis (14). This provided a major advantage in that the quantitative agreement of our results with Equation 2 demonstrates that each identified locus is functionally relevant. This overcomes a common limitation of binding assays between channel fragments, which may identify sites that are inaccessible or inconsequential in the context of the holochannel. Moreover, by fitting to a specific Langmuir curve, we can distinguish mutations that may alter

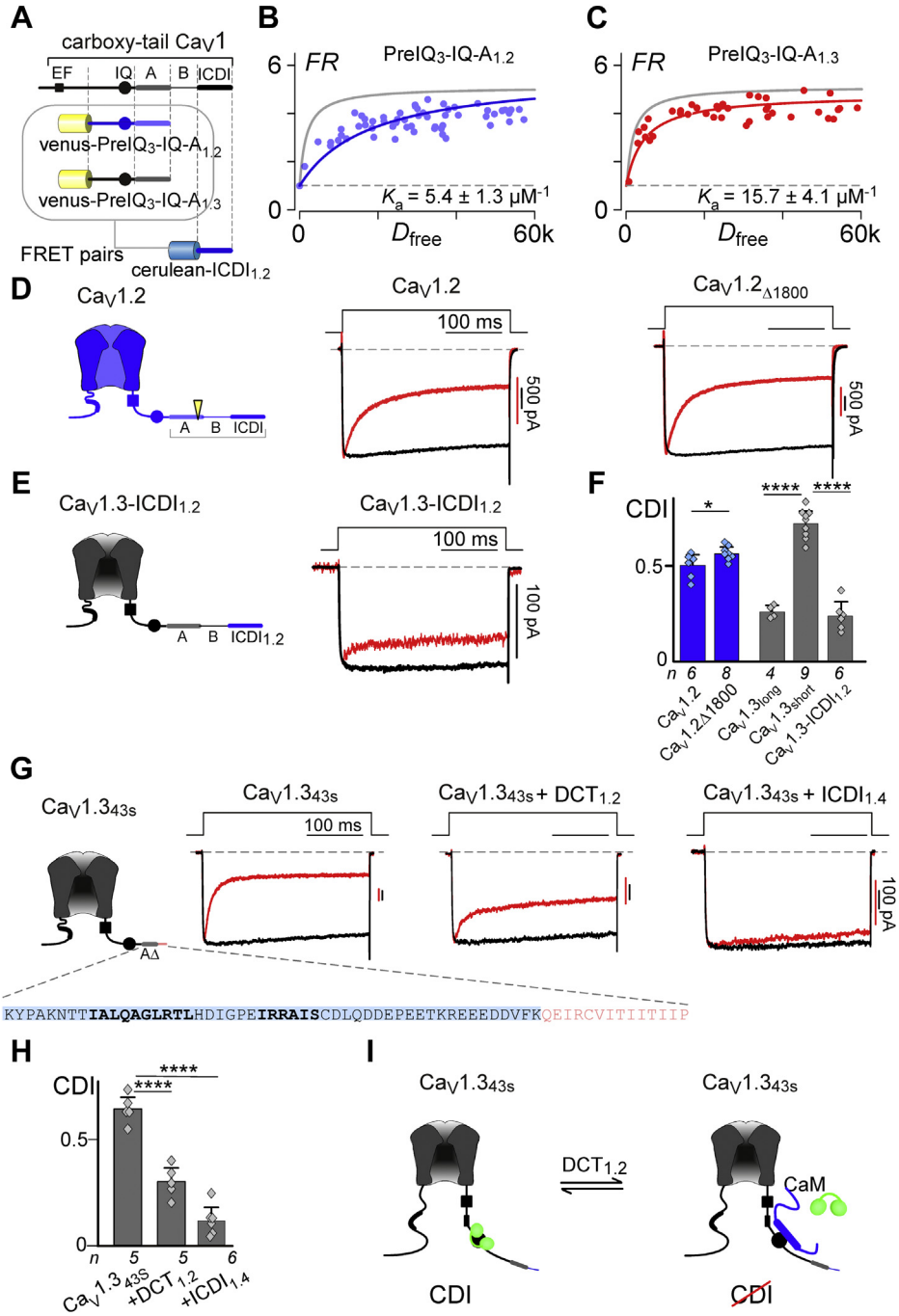


**Figure 4. Residual functionality of ICDI1.2 in modulating $Ca_V$ channels.** *A*, cartoon depicting FRET interacting pairs for panels *B* and *C*. Venus-PreIQ$_3$-IQ-A$_{1.2}$ or Venus-PreIQ$_3$-IQ-A$_{1.3}$ was paired with Cerulean-ICDI$_{1.2}$ in order to evaluate the role of the ICDI contained within $Ca_V$1.2 channels. *B*, Venus-PreIQ$_3$-IQ-A$_{1.2}$ displays moderate binding with Cerulean-ICDI$_{1.2}$ (*blue*) as compared with the robust binding between Venus-PreIQ$_3$-IQ-A$_{1.3}$ and Cerulean-ICDI$_{1.4}$ which is reproduced as the *gray line* for comparison. *C*, Venus-PreIQ$_3$-IQ-A$_{1.3}$ is able to bind strongly with Cerulean-ICDI$_{1.2}$. *D*, *Left*, channel cartoon with cleavage site indicated by the *yellow arrowhead*. *Right*, exemplar data demonstrating that truncation of $Ca_V$1.2 at the cleavage site has a minor effect on CDI. *E*, *Left*, channel cartoon indicating introduction of ICDI$_{1.2}$ into the $Ca_V$1.3 channel backbone. *Right*, introduction of ICDI$_{1.2}$ into $Ca_V$1.3 channels causes a large decrease in CDI. *F*, average CDI data demonstrating a modest but statistically significant effect of ICDI$_{1.2}$ on $Ca_V$1.2 channels (*blue*), and a large effect on $Ca_V$1.3, which is comparable to the native effect of ICDI$_{1.3}$ contained within $Ca_V$1.3$_{long}$ (*gray*). Data are plotted as mean ± SD. ($Ca_V$1.2: *$p < 0.05$ based on a Student's *t*-test; $Ca_V$1.3: ANOVA summary analysis indicates a likelihood of significant difference at a level of $p < 0.0001$. Post-hoc Dunnett's multiple comparisons *versus* $Ca_V$1.3$_{short}$ indicated as ****$p < 0.0001$.) *G*, *Left*, cartoon of human $Ca_V$1.3$_{43S}$, with the sequence of the end of the channel displayed below. This splice variant contains a portion of the A region (*blue highlight*), which contains the identified hotspots required for ICDI binding (*bold*), as well as a short sequence of unique amino acids prior to truncation of the channel (*pink*). *Right*, exemplar whole-cell patch clamp data demonstrates robust CDI in WT $Ca_V$1.3$_{43S}$, which is reduced when the predicted cleavage fragment of the human $Ca_V$1.2 channel is coexpressed, or when ICDI$_{1.4}$ is expressed as a peptide. *H*, average CDI effects for the channels described in panel *G*, DCT$_{1.2}$ and ICDI$_{1.4}$ both have significant effects on the CDI of $Ca_V$1.3$_{43S}$ (ANOVA summary analysis indicates a likelihood of significant difference at a level of $p < 0.0001$. Post-hoc Dunnett's multiple comparisons *versus* $Ca_V$1.3$_{43s}$ indicated as ****$p < 0.0001$; data are displayed ±SD). *I*, cartoon proposing a cross-channel effect of ICDI$_{1.2}$, such that cleaved or independently transcribed DCT$_{1.2}$ may modulate $Ca_V$1.3$_{43S}$ channels.

channel function through ancillary mechanisms such as transduction or altered folding of the channel. Thus, in addition to identifying critical loci, our results confirm the competitive mechanism described for ICDI modulation of CDI.

A number of previous studies have identified regions within the carboxy tail of $Ca_V1$ channels, which are critical to the competitive mechanism of ICDI inhibition. Among these are the PCRD and DCRD regions, which were identified within $Ca_V1.2$ channels as potential interaction sites such that the DCRD region of the proteolytically cleaved $Ca_V1.2$ DCT may interact with the PCRD on the channel *via* electrostatic interaction with the negatively charged amino acids (33). Homologous regions within $Ca_V1.3$ and $Ca_V1.4$ were later shown to be important for ICDI regulation and for the interaction with modular peptides (27, 30, 31, 33, 47). In this study, the PCRD resides within the A region and overlaps with the identified locus of critical amino acids required for high-affinity binding between the IQ-A and ICDI. Interestingly, these critical amino acids were identified both within the PCRD and upstream of the motif, arguing for a larger interacting region, which is highly conserved across $Ca_V$ channels (Fig. S8). However, our binding assay also demonstrated that the A region, in itself, is insufficient for high-affinity binding, but also requires the upstream IQ region (Fig. 3*A*). This fits with previous findings in which neutralization of the PCRD arginines was not sufficient to prevent the ICDI inhibition of CDI (31), pointing to the existence of additional interaction loci. In a similar manner, our scan of the ICDI region validated the importance of the DCRD, while also identifying numerous critical interacting loci upstream of the motif (Fig. S8). Thus, this study has expanded our knowledge of the important interactions required for ICDI inhibition, providing a comprehensive map of the critical loci within the carboxy tail.

The impact of ICDI in $Ca_V1.3$ and $Ca_V1.4$ channels has been well recognized; however, its role in $Ca_V1.2$ has been uncertain. It has been demonstrated that the truncation of $Ca_V1.2$ results in increased current density, altered voltage dependence of channel activation, and disrupted targeting of the channel to the membrane (33, 53, 54); however, no impact on CDI has been reported. Here, we find that the impact of $ICDI_{1.2}$ within $Ca_V1.2$ channels is minimal, allowing cleavage of this DCT region without significant disruption of CDI. Yet $ICDI_{1.2}$ is capable of causing significant disruption of CDI in the context of $Ca_V1.3$ (Fig. 4, *E–I*) (27). This selective effect of $ICDI_{1.2}$ on $Ca_V1.3$ channels is intriguing as it represents a difficult to achieve discrimination between $Ca_V1.2$ and $Ca_V1.3$ (55, 56). The strong homology between these two channels has resulted in challenges to dissecting the contribution of each channel to the function of cells, which express both channel subtypes, and hinders therapeutic options for neuropsychiatric disorders, which may benefit from blockade of $Ca_V1.3$ (55). As such, the interface defined in this study between the IQ-A region and ICDI may represent a promising interface with which to selectively target $Ca_V1.3$.

The DCT of $Ca_V1.2$ is routinely cleaved in neurons and myocytes, with the cleavage product able to either remain associated with the channel (33) or translocate to the nucleus (41). Our FRET binding data would argue that this association between $Ca_V1.2$ and the DCT may be relatively weak, leaving $DCT_{1.2}$ available to other binding partners. Moreover, it has been shown that an alternate start site exists within the carboxy tail of $Ca_V1.2$, such that alternative transcription of $Ca_V1.2$ will produce a DCT peptide containing a calcium channel-associated transcription regulator (CCAT) (41). Importantly, ICDI would be intact within this peptide, providing an additional source of $DCT_{1.2}$ within cells. In addition, CCAT has been shown to localize to the cytosol in a $Ca^{2+}$-dependent manner, providing a source of ICDI in proximity to the membrane, which can be tuned by activity (41). Our FRET binding analysis (Fig. 4*A*) suggests that the $Ca_V1.2$ DCT is capable of binding upstream calmodulatory elements in $Ca_V1.2$, albeit weakly. Functional analysis, however, suggests only minimal effects of this segment on $Ca_V1.2$ CDI. By comparison, the $Ca_V1.3_{43S}$ channel variant contains all the elements required for high-affinity binding with $DCT_{1.2}$ and exhibits functional inhibition of CDI (Fig. 4*G*), consistent with previous studies (27). Moreover, $Ca_V1.3_{43S}$ is widely expressed in the brain, accounting for up to 39% of transcripts, and is often expressed within the same neuron type as $Ca_V1.2$ (27). Thus, it seems likely that $DCT_{1.2}$ may interact with this channel, altering the normally robust CDI. It is interesting to note, however, that while $DCT_{1.2}$ is poised to modulate some $Ca_V1.3$ channels, the same cannot be said of $DCT_{1.3}$. Not only is the IQ-A region of $Ca_V1.2$ suboptimal for binding to ICDI, but there is little evidence that $Ca_V1.3$ is cleaved in neurons (31). Thus, this cross-channel modulation may be unidirectional. Finally, since $Ca_V1.2$ and $Ca_V1.3$ often exist within the same neuron, this mode of cross-channel modulation may represent an important method for tuning CDI in different regions of the brain.

## Experimental procedures

### *Molecular biology*

The rat brain $Ca_V1.3$ α1 subunit (in pcDNA6) corresponds to AF370009.1 (57) and was incorporated to the mammalian expression plasmid pCDNA6 (Invitrogen) (20). This plasmid features a unique *Bgl*II restriction site at a locus corresponding to ∼450 amino acids upstream of the IQ domain and a unique *Xba*I site after the stop codon, which were used for generation of mutant and chimeric plasmids as descried below. The $Ca_V1.2$ α1 subunit (in pGW) is identical to rabbit NM001136522 (58), and the $Ca_V1.4$ channel (in pcDNA3) is the human clone corresponding to NP005174.2. $Ca_V1.3_{\Delta/DCT1.4}$ was made by fusing with the DCT of the $Ca_V1.4$ α1 subunit to the $Ca_V1.3$ α1 subunit (truncated after the IQ domain), as previously described (20). $Ca_V1.3_{43S}$ was made by PCR amplification of the channel segment between the *Bgl*II site and IQ domain with the appendage of amino acids unique to this splice variant (27). The PCR product was then inserted into the channel *via* the *Bgl*II/*Xba*I sites.

FRET constructs were fluorescent-tagged (either Venus or Cerulean) using similar strategies as previously described (45).

Briefly, Venus and Cerulean fluorophores (a kind gift from Dr Steven Vogel, NIH) were subcloned into the pcDNA3 vector *via* unique *Kpn*I and *Not*I sites. The PCR-amplified channel peptides, as described in Liu *et al.*, (20) were then cloned *via* unique *Not*I and *Xba*I sites. Mutations were introduced into the channel or FRET construct *via* PCR amplification or overlap extension PCR.

### Transfection of HEK293 cells

For electrophysiology experiments, HEK293 cells were cultured on 10-cm plates, and channels were transiently transfected by a calcium phosphate protocol (10). We applied 8 μg of plasmid DNA encoding the desired pore forming α1 subunit, as well as 8 μg of $\beta_{2A}$ (M80545) and 8 μg of rat $\alpha_{2\delta}$ (NM012919.2) subunits along with 3 μg of SV40 T antigen. For microscope-based FRET assays, HEK293 cells cultured on 3.5-cm culture dishes with integral No. 0 glass coverslip bottoms (*In Vitro* Scientific) were transiently transfected using polyethylenimine (PEI) reagent (Polysciences).

### Whole-cell patch clamp recordings

Whole-cell recordings were obtained using an Axopatch 200A amplifier (Axon Instruments). Electrodes were pulled from borosilicate glass capillaries (World Precision Instruments), with 1 to 3 MΩ resistances, which were in turn compensated for series resistance by >60%. Currents were low-pass filtered at 2 kHz before digital acquisition at five times the frequency. A P/8 leak subtraction protocol was used. The internal solution contained (in mM): CsMeSO3, 114; CsCl, 5; MgATP, 4; HEPES (pH 7.4), 10; and BAPTA (1,2-bis(*o*-aminophenoxy)ethane- *N,N,N′,N′*-tetraacetic acid), 10; at 295 mOsm adjusted with CsMeSO3. The bath solution contained (in mM): TEA-MeSO3, 102; HEPES (pH 7.4), 10; CaCl2 or BaCl2, 40; at 305 mOsm adjusted with TEA-MeSO3. Data was analyzed using custom Matlab scripts. Inactivation was quantified as the ratio of current remaining after 300 ms (current amplitude measured at 300 ms divided by peak current amplitude) in either $Ca^{2+}$ or $Ba^{2+}$ ($r_{300}$). CDI was then quantified as the $r_{300}$ in $Ca^{2+}$ subtracted from the $r_{300}$ in $Ba^{2+}$, measured at 10 mV for $Ca_V1.3$ channels, and 30 mV for $Ca_V1.2$.

### FRET optical imaging

FRET two-hybrid experiments were performed on an inverted microscope as described (45, 46). The bath solution was a Tyrode's solution composed of (in mM): NaCl, 138; KCl, 4; MgCl2, 1; HEPES (pH 7.4), 10; CaCl2, 2; at 305 mOsm adjusted with glucose. Background fluorescent signals were measured from cells without expression of the fluorophores and subtracted from cells expressing the fluorophores. Concentration-dependent spurious FRET was subtracted from the raw data prior to binding-curve analysis (45, 46). Cerulean (59) and Venus (60) were used as the donor and acceptor fluorescent proteins instead of eCFP and eYFP, as their optical properties provided more robust and stable FRET signals. Acceptor-centric measurements of FRET were obtained with the $3^3$-FRET algorithm (45, 46), in which the effective FRET efficiency ($E_{EFF}$) and FRET ratio ($FR$) are defined as:

$$E_{Eff} = E \times A_b = (FR - 1)[\varepsilon_{Ven(440\ nm)} / \varepsilon_{Cer(440\ nm)}] \quad (3)$$

where $E$ is the FRET efficiency of a donor–acceptor pair, $A_b$ is the fraction of acceptor molecules bound by a donor, and $\varepsilon_{Ven(440\ nm)}/\varepsilon_{Cer(440\ nm)}$ is the approximate molar extinction coefficients of Cerulean and Venus, which was measured as 0.08 on our setup. Intensity measurements at each wavelength were taken from individual cells such that variable expression across the cells enabled population of a binding curve. Binding curves were analyzed using GraphPad software (Prism), providing relative $K_d$ values and standard error based on an unbiased fit to the data. These relative $K_d$ values were then calibrated according to a previously determined calibration factor (13, 20) and converted to $K_a = 1/K_d$. Importantly, the previous calibration factor determined for our setup utilized CFP/YFP FRET pairs. In order to account for the difference in FR using Cerulean and Venus, we determined the relative $K_d$ for multiple peptides using both the fluorophore pairs and found that the two data sets differed by a factor of 1.8, which we incorporated into the calibration factor.

## Data availability

All data is contained within the article.

*Supporting information*—This article contains supporting information (13, 14, 20, 33, 43, 49).

*Acknowledgments*—This project was initiated under the direction of Dr David Yue, who passed away in 2014. David was a brilliant scientist and exceptional mentor, and we are grateful for his guidance and friendship. We would like to thank Dr Gordon Tomaselli for his guidance and support. We would also like to thank Hojjat Bazzazi for providing FRET plasmids and for useful discussion and advice throughout the project. In addition, we thank Wanjun Yang for dedicated technical support and thank members of the Calcium Signals lab at Johns Hopkins for discussion and support of this project, as well as members of Dr Dick's lab at the University of Maryland for insightful discussions and editing of the manuscript.

*Author contributions*—L. J. S., D. T. Y., M. B. -J., and I. E. D. designed the study; L. J. S., D. C. O. V., M. B. -J., and I. E. D. performed the experiments; L. J. S., D. C. O. V., D. T. Y., M. B. -J., and I. E. D. analyzed the data and designed the figures; and L. J. S., and I. E. D. wrote the paper with input and edits from all the authors.

*Funding and additional information*—This grant was supported by an NIH/NINDS grant 5R01NS085074 and by an NIH/NHLBI grant 1R01HL149926. The content is solely the responsibility of the authors and does not necessarily represent the official views of the National Institutes of Health.

*Conflict of interest*—The authors declare that they have no conflicts of interest with the contents of this article.

*Abbreviations*—The abbreviations used are: apoCaM, $Ca^{2+}$ free calmodulin; $Ca^{2+}$, calcium; CaM, calmodulin; $Ca_V$, voltage-gated

calcium channel; CDI, calcium/CaM-dependent inactivation; CFP, cyan fluorescent protein; DCRD, distal C-terminal regulatory domain; DCT, distal carboxy tail; FR, fret ratio; FRET, fluorescence resonance energy transfer; ICDI, inhibitor of CDI; iTL, individually transformed Langmuir; PCRD, proximal C-terminal regulatory domain; YFP, yellow fluorescent protein.

## References


1. Harvey, R. D., and Hell, J. W. (2013) CaV1.2 signaling complexes in the heart. *J. Mol. Cell. Cardiol.* **58**, 143–152
2. Gutierrez, L. M., Brawley, R. M., and Hosey, M. M. (1991) Dihydropyridine-sensitive calcium channels from skeletal muscle. I. Roles of subunits in channel activity. *J. Biol. Chem.* **266**, 16387–16394
3. Striessnig, J., Koschak, A., Sinnegger-Brauns, M. J., Hetzenauer, A., Nguyen, N. K., Busquet, P., Pelster, G., and Singewald, N. (2006) Role of voltage-gated L-type Ca2+ channel isoforms for brain function. *Biochem. Soc. Trans.* **34**, 903–909
4. Lipscombe, D., Helton, T. D., and Xu, W. (2004) L-type calcium channels: The low down. *J. Neurophysiol.* **92**, 2633–2641
5. McDonald, T. F., Pelzer, S., Trautwein, W., and Pelzer, D. J. (1994) Regulation and modulation of calcium channels in cardiac, skeletal, and smooth muscle cells. *Physiol. Rev.* **74**, 365–507
6. Ghosh, D., Syed, A. U., Prada, M. P., Nystoriak, M. A., Santana, L. F., Nieves-Cintron, M., and Navedo, M. F. (2017) Calcium channels in vascular smooth muscle. *Adv. Pharmacol.* **78**, 49–87
7. Liang, H., DeMaria, C. D., Erickson, M. G., Mori, M. X., Alseikhan, B. A., and Yue, D. T. (2003) Unified mechanisms of $Ca^{2+}$ regulation across the $Ca^{2+}$ channel family. *Neuron* **39**, 951–960
8. Pitt, G. S., Zuhlke, R. D., Hudmon, A., Schulman, H., Reuter, H., and Tsien, R. W. (2001) Molecular basis of calmodulin tethering and Ca2+-dependent inactivation of L-type Ca2+ channels. *J. Biol. Chem.* **276**, 30794–30802
9. Alseikhan, B. A., DeMaria, C. D., Colecraft, H. M., and Yue, D. T. (2002) Engineered calmodulins reveal the unexpected eminence of Ca2+ channel inactivation in controlling heart excitation. *Proc. Natl. Acad. Sci. U. S. A.* **99**, 17185–17190
10. Peterson, B. Z., DeMaria, C. D., Adelman, J. P., and Yue, D. T. (1999) Calmodulin is the $Ca^{2+}$ sensor for Ca2+ -dependent inactivation of L-type calcium channels. *Neuron* **22**, 549–558
11. Zuhlke, R. D., Pitt, G. S., Deisseroth, K., Tsien, R. W., and Reuter, H. (1999) Calmodulin supports both inactivation and facilitation of L-type calcium channels. *Nature* **399**, 159–162
12. Adams, P. J., Ben-Johny, M., Dick, I. E., Inoue, T., and Yue, D. T. (2014) Apocalmodulin itself promotes ion channel opening and Ca(2+) regulation. *Cell* **159**, 608–622
13. Bazzazi, H., Ben Johny, M., Adams, P. J., Soong, T. W., and Yue, D. T. (2013) Continuously tunable Ca(2+) regulation of RNA-edited CaV1.3 channels. *Cell Rep.* **5**, 367–377
14. Ben Johny, M., Yang, P. S., Bazzazi, H., and Yue, D. T. (2013) Dynamic switching of calmodulin interactions underlies Ca2+ regulation of CaV1.3 channels. *Nat. Commun.* **4**, 1717
15. Splawski, I., Timothy, K. W., Decher, N., Kumar, P., Sachse, F. B., Beggs, A. H., Sanguinetti, M. C., and Keating, M. T. (2005) Severe arrhythmia disorder caused by cardiac L-type calcium channel mutations. *Proc. Natl. Acad. Sci. U. S. A.* **102**, 8089–8096. discussion 8086-8088
16. Splawski, I., Timothy, K. W., Sharpe, L. M., Decher, N., Kumar, P., Bloise, R., Napolitano, C., Schwartz, P. J., Joseph, R. M., Condouris, K., Tager-Flusberg, H., Priori, S. G., Sanguinetti, M. C., and Keating, M. T. (2004) Ca(V)1.2 calcium channel dysfunction causes a multisystem disorder including arrhythmia and autism. *Cell* **119**, 19–31
17. Griessmeier, K., Cuny, H., Roetzer, K., Griesbeck, O., Harz, H., Biel, M., and Wahl-Schott, C. (2009) Calmodulin is a functional regulator of $Ca_V1.4$ l-type $Ca^{2+}$ channels. *J. Biol. Chem.* **284**, 29809–29816
18. Haeseleer, F., Williams, B., and Lee, A. (2016) Characterization of C-terminal splice variants of Cav1.4 Ca2+ channels in human retina. *J. Biol. Chem.* **291**, 15663–15673
19. Yang, P. S., Alseikhan, B. A., Hiel, H., Grant, L., Mori, M. X., Yang, W., Fuchs, P. A., and Yue, D. T. (2006) Switching of $Ca^{2+}$-dependent inactivation of $Ca_V1.3$ channels by calcium binding proteins of auditory hair cells. *J. Neurosci.* **26**, 10677–10689
20. Liu, X., Yang, P. S., Yang, W., and Yue, D. T. (2010) Enzyme-inhibitor-like tuning of Ca(2+) channel connectivity with calmodulin. *Nature* **463**, 968–972
21. Yang, P. S., Johny, M. B., and Yue, D. T. (2014) Allostery in Ca(2)(+) channel modulation by calcium-binding proteins. *Nat. Chem. Biol.* **10**, 231–238
22. Shaltiel, L., Paparizos, C., Fenske, S., Hassan, S., Gruner, C., Rotzer, K., Biel, M., and Wahl-Schott, C. A. (2012) Complex regulation of voltage-dependent activation and inactivation properties of retinal voltage-gated Cav1.4 L-type Ca2+ channels by Ca2+-binding protein 4 (CaBP4). *J. Biol. Chem.* **287**, 36312–36321
23. Campiglio, M., Coste de Bagneaux, P., Ortner, N. J., Tuluc, P., Van Petegem, F., and Flucher, B. E. (2018) STAC proteins associate to the IQ domain of CaV1.2 and inhibit calcium-dependent inactivation. *Proc. Natl. Acad. Sci. U. S. A.* **115**, 1376–1381
24. Niu, J., Dick, I. E., Yang, W., Bamgboye, M. A., Yue, D. T., Tomaselli, G., Inoue, T., and Ben-Johny, M. (2018) Allosteric regulators selectively prevent Ca(2+)-feedback of CaV and NaV channels. *Elife* **7**, e35222
25. Polster, A., Dittmer, P. J., Perni, S., Bichraoui, H., Sather, W. A., and Beam, K. G. (2018) Stac proteins suppress Ca(2+)-dependent inactivation of neuronal l-type Ca(2+) channels. *J. Neurosci.* **38**, 9215–9227
26. Wong King Yuen, S. M., Campiglio, M., Tung, C. C., Flucher, B. E., and Van Petegem, F. (2017) Structural insights into binding of STAC proteins to voltage-gated calcium channels. *Proc. Natl. Acad. Sci. U. S. A.* **114**, E9520–E9528
27. Bock, G., Gebhart, M., Scharinger, A., Jangsangthong, W., Busquet, P., Poggiani, C., Sartori, S., Mangoni, M. E., Sinnegger-Brauns, M. J., Herzig, S., Striessnig, J., and Koschak, A. (2011) Functional properties of a newly identified C-terminal splice variant of Cav1.3 L-type Ca2+ channels. *J. Biol. Chem.* **286**, 42736–42748
28. Tan, G. M., Yu, D., Wang, J., and Soong, T. W. (2012) Alternative splicing at C-terminus of CaV1.4 calcium channel modulates calcium-dependent inactivation, activation potential and current density. *J. Biol. Chem.* **287**, 832–847
29. Wahl-Schott, C., Baumann, L., Cuny, H., Eckert, C., Griessmeier, K., and Biel, M. (2006) Switching off calcium-dependent inactivation in L-type calcium channels by an autoinhibitory domain. *Proc. Natl. Acad. Sci. U. S. A.* **103**, 15657–15662
30. Lieb, A., Scharinger, A., Sartori, S., Sinnegger-Brauns, M. J., and Striessnig, J. (2012) Structural determinants of CaV1.3 L-type calcium channel gating. *Channels (Austin)* **6**, 197–205
31. Singh, A., Gebhart, M., Fritsch, R., Sinnegger-Brauns, M. J., Poggiani, C., Hoda, J. C., Engel, J., Romanin, C., Striessnig, J., and Koschak, A. (2008) Modulation of voltage- and $Ca^{2+}$-dependent gating of $Ca_V1.3$ L-type calcium channels by alternative splicing of a C-terminal regulatory domain. *J. Biol. Chem.* **283**, 20733–20744
32. Singh, A., Hamedinger, D., Hoda, J. C., Gebhart, M., Koschak, A., Romanin, C., and Striessnig, J. (2006) C-terminal modulator controls $Ca^{2+}$-dependent gating of $Ca_V1.4$ L-type $Ca^{2+}$ channels. *Nat. Neurosci.* **9**, 1108–1116
33. Hulme, J. T., Yarov-Yarovoy, V., Lin, T. W., Scheuer, T., and Catterall, W. A. (2006) Autoinhibitory control of the CaV1.2 channel by its proteolytically processed distal C-terminal domain. *J. Physiol.* **576**, 87–102
34. Christel, C. J., Cardona, N., Mesirca, P., Herrmann, S., Hofmann, F., Striessnig, J., Ludwig, A., Mangoni, M. E., and Lee, A. (2012) Distinct localization and modulation of Cav1.2 and Cav1.3 L-type Ca2+ channels in mouse sinoatrial node. *J. Physiol.* **590**, 6327–6342
35. Mangoni, M. E., Couette, B., Bourinet, E., Platzer, J., Reimer, D., Striessnig, J., and Nargeot, J. (2003) Functional role of L-type Cav1.3 Ca2+ channels in cardiac pacemaker activity. *Proc. Natl. Acad. Sci. U. S. A.* **100**, 5543–5548
36. Huang, H., Tan, B. Z., Shen, Y., Tao, J., Jiang, F., Sung, Y. Y., Ng, C. K., Raida, M., Kohr, G., Higuchi, M., Fatemi-Shariatpanahi, H., Harden, B., Yue, D. T., and Soong, T. W. (2012) RNA editing of the IQ domain in

Ca(v)1.3 channels modulates their Ca(2)(+)-dependent inactivation. *Neuron* **73**, 304–316
37. Bezprozvanny, I. (2009) Calcium signaling and neurodegenerative diseases. *Trends Mol. Med.* **15**, 89–100
38. Hurley, M. J., Brandon, B., Gentleman, S. M., and Dexter, D. T. (2013) Parkinson's disease is associated with altered expression of CaV1 channels and calcium-binding proteins. *Brain* **136**, 2077–2097
39. Hoda, J. C., Zaghetto, F., Koschak, A., and Striessnig, J. (2005) Congenital stationary night blindness type 2 mutations S229P, G369D, L1068P, and W1440X alter channel gating or functional expression of Ca(v)1.4 L-type Ca2+ channels. *J. Neurosci.* **25**, 252–259
40. Strom, T. M., Nyakatura, G., Apfelstedt-Sylla, E., Hellebrand, H., Lorenz, B., Weber, B. H., Wutz, K., Gutwillinger, N., Ruther, K., Drescher, B., Sauer, C., Zrenner, E., Meitinger, T., Rosenthal, A., and Meindl, A. (1998) An L-type calcium-channel gene mutated in incomplete X-linked congenital stationary night blindness. *Nat. Genet.* **19**, 260–263
41. Gomez-Ospina, N., Tsuruta, F., Barreto-Chang, O., Hu, L., and Dolmetsch, R. (2006) The C terminus of the L-type voltage-gated calcium channel Ca(V)1.2 encodes a transcription factor. *Cell* **127**, 591–606
42. Schroder, E., Byse, M., and Satin, J. (2009) L-type calcium channel C terminus autoregulates transcription. *Circ. Res.* **104**, 1373–1381
43. Sang, L., Dick, I. E., and Yue, D. T. (2016) Protein kinase A modulation of CaV1.4 calcium channels. *Nat. Commun.* **7**, 12239
44. Doering, C. J., Hamid, J., Simms, B., McRory, J. E., and Zamponi, G. W. (2005) Cav1.4 encodes a calcium channel with low open probability and unitary conductance. *Biophys. J.* **89**, 3042–3048
45. Erickson, M. G., Alseikhan, B. A., Peterson, B. Z., and Yue, D. T. (2001) Preassociation of calmodulin with voltage-gated Ca(2+) channels revealed by FRET in single living cells. *Neuron* **31**, 973–985
46. Erickson, M. G., Liang, H., Mori, M. X., and Yue, D. T. (2003) FRET two-hybrid mapping reveals function and location of L-type Ca2+ channel CaM preassociation. *Neuron* **39**, 97–107
47. Liu, N., Yang, Y., Ge, L., Liu, M., Colecraft, H. M., and Liu, X. (2017) Cooperative and acute inhibition by multiple C-terminal motifs of L-type Ca(2+) channels. *Elife* **6**, e21989
48. Fuller, M. D., Emrick, M. A., Sadilek, M., Scheuer, T., and Catterall, W. A. (2010) Molecular mechanism of calcium channel regulation in the fight-or-flight response. *Sci. Signal.* **3**, ra70
49. Hulme, J. T., Konoki, K., Lin, T. W., Gritsenko, M. A., Camp, D. G., Bigelow, D. J., and Catterall, W. A. (2005) Sites of proteolytic processing and noncovalent association of the distal C-terminal domain of CaV1.1 channels in skeletal muscle. *Proc. Natl. Acad. Sci. U. S. A.* **102**, 5274–5279
50. Chaudhuri, D., Issa, J. B., and Yue, D. T. (2007) Elementary mechanisms producing facilitation of Cav2.1 (P/Q-type) channels. *J. Gen. Physiol.* **129**, 385–401
51. Kim, J., Ghosh, S., Nunziato, D. A., and Pitt, G. S. (2004) Identification of the components controlling inactivation of voltage-gated $Ca^{2+}$ channels. *Neuron* **41**, 745–754
52. Lee, A., Zhou, H., Scheuer, T., and Catterall, W. A. (2003) Molecular determinants of Ca(2+)/calmodulin-dependent regulation of Ca(v)2.1 channels. *Proc. Natl. Acad. Sci. U. S. A.* **100**, 16059–16064
53. Gerhardstein, B. L., Gao, T., Bunemann, M., Puri, T. S., Adair, A., Ma, H., and Hosey, M. M. (2000) Proteolytic processing of the C terminus of the alpha(1C) subunit of L-type calcium channels and the role of a proline-rich domain in membrane tethering of proteolytic fragments. *J. Biol. Chem.* **275**, 8556–8563
54. Gao, T., Bunemann, M., Gerhardstein, B. L., Ma, H., and Hosey, M. M. (2000) Role of the C terminus of the alpha 1C (CaV1.2) subunit in membrane targeting of cardiac L-type calcium channels. *J. Biol. Chem.* **275**, 25436–25444
55. Striessnig, J., Ortner, N. J., and Pinggera, A. (2015) Pharmacology of L-type calcium channels: Novel drugs for old targets? *Curr. Mol. Pharmacol.* **8**, 110–122
56. Huang, H., Ng, C. Y., Yu, D., Zhai, J., Lam, Y., and Soong, T. W. (2014) Modest CaV1.342-selective inhibition by compound 8 is beta-subunit dependent. *Nat. Commun.* **5**, 4481
57. Xu, W., and Lipscombe, D. (2001) Neuronal Ca(V)1.3alpha(1) L-type channels activate at relatively hyperpolarized membrane potentials and are incompletely inhibited by dihydropyridines. *J. Neurosci.* **21**, 5944–5951
58. Wei, X. Y., Perez-Reyes, E., Lacerda, A. E., Schuster, G., Brown, A. M., and Birnbaumer, L. (1991) Heterologous regulation of the cardiac Ca2+ channel alpha 1 subunit by skeletal muscle beta and gamma subunits. Implications for the structure of cardiac L-type Ca2+ channels. *J. Biol. Chem.* **266**, 21943–21947
59. Rizzo, M. A., Springer, G. H., Granada, B., and Piston, D. W. (2004) An improved cyan fluorescent protein variant useful for FRET. *Nat. Biotechnol.* **22**, 445–449
60. Nagai, T., Ibata, K., Park, E. S., Kubota, M., Mikoshiba, K., and Miyawaki, A. (2002) A variant of yellow fluorescent protein with fast and efficient maturation for cell-biological applications. *Nat. Biotechnol.* **20**, 87–90